Supplementary Information

Manuscript title:
Electrically Reconfigurable Polarization Control with Double Tri-Layer Black Phosphorus Heterostructures

Authors:
Samuel K.W. Seah, Souvik Biswas, Claudio U. Hail, George R. Rossman, Harry A. Atwater

Number of supplementary pages:
21

Number of supplementary notes:
18

Supplementary Note 1. Effect of top PMMA layer on cavity resonant wavelength

Since the cavity resonant wavelength was predominantly determined by the hBN thicknesses which could not be changed post-transfer, an alternative method was devised to impart some tunability to the device. Spinning PMMA on top of the Fabry-Perot structure allowed it to function as a Salisbury screen that could couple part of the Fabry-Perot mode out of the partially transmissive top gold mirror (Supplementary Fig. 1a). Since the PMMA could be washed off during fabrication without affecting the heterostructure underneath, this allowed for some cavity resonance wavelength tunability (Supplementary Fig. 1b).

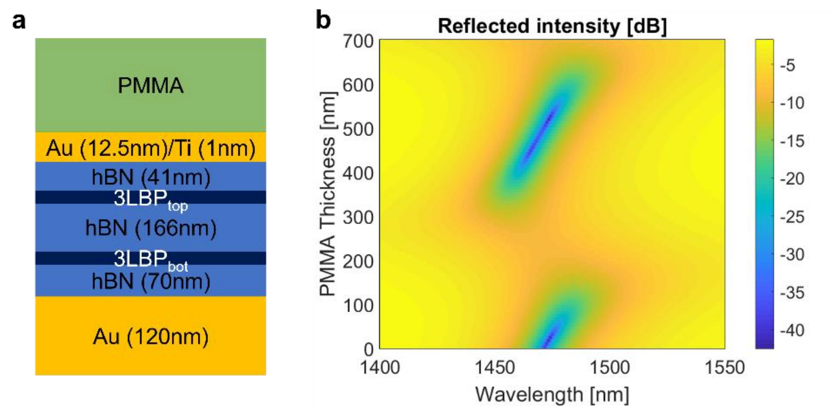

Supplementary Fig. 1. (**a**) Schematic of the simulated dual-gated device. (**b**) Simulated reflection intensity map of the dual-gated device as a function of top PMMA thickness and operating wavelength, in the absence of any gating.

Supplementary Note 2. Optical image of dual-gated device with full annotations

During fabrication, great care was taken to electrically connect the BP flakes to the side gold fingers, while still encapsulating the BP with hBN to prevent oxidation (Supplementary Fig. 2). The bottom 3L-BP flake was connected to a 6-layer BP piece from exfoliation. Both the 3L and 6L parts were picked up during the transfer, with the entirety of the BP flake being covered on top with hBN. The 6L-BP part was then exposed to the gold finger from its underside. For the top 3L-BP flake, an additional piece of graphene had to be picked up to electrically contact the top gold finger.

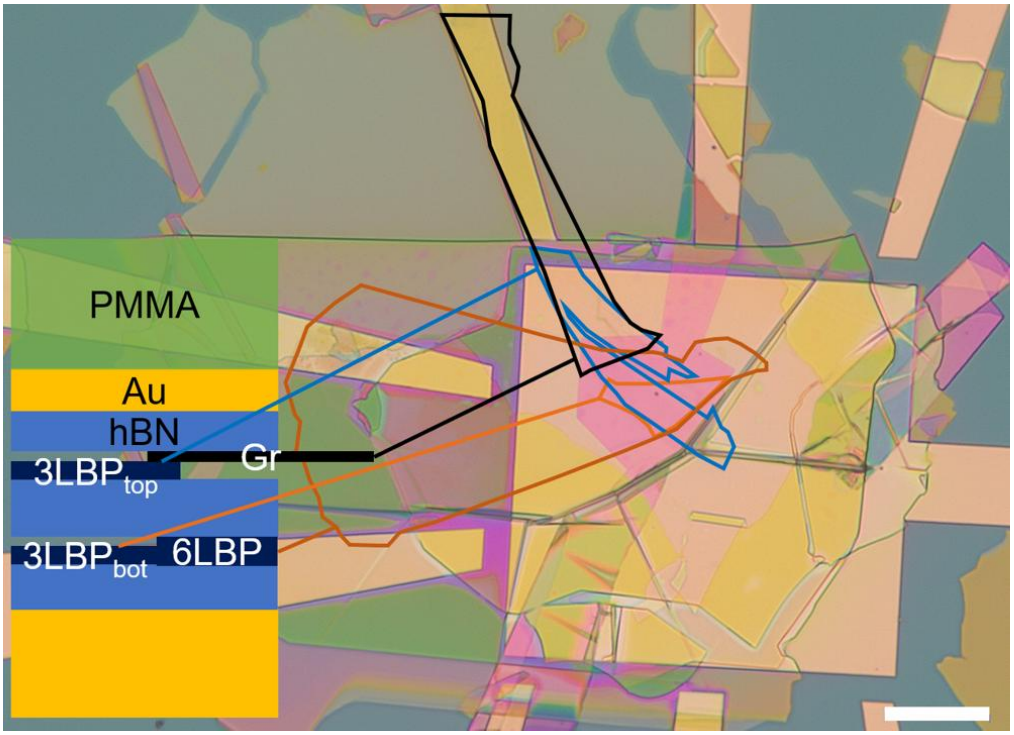

Supplementary Fig. 2. Optical image of the dual-gated device, with border outlines of the 3L-BP, 6L-BP, and graphene (Gr) layers showing their electrical connections to the gold fingers for gating. The white bar represents 20μm. (Inset) Schematic of the heterostructure and the relevant layers marked on the optical image.

Supplementary Note 3. Spectral reflectance as a function of input polarization angle

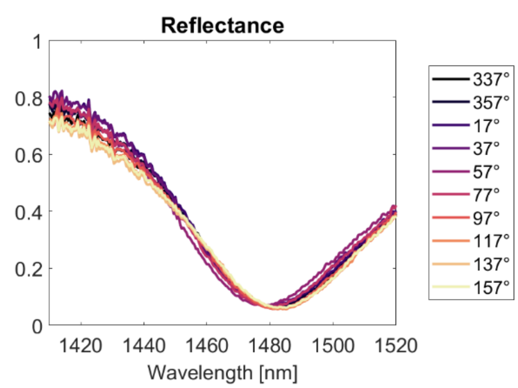

Supplementary Fig. 3. Normalized spectral reflectance of dual-gated device near the center of the overlapping region of the top and bottom 3L-BP layers, as a function of input linear polarization angle. The angle values are with respect to the horizontal of the optical image shown in Fig. 3a.

Supplementary Note 4. Stokes parameter maps as a function of gating voltage and operating wavelength

On the pixel of interest marked in Fig. 3d, a full voltage & wavelength sweep was done to probe changes in the Stokes parameters (Supplementary Fig. 4). Top and bottom gating voltages were separately swept from 0 V, to the maximum voltage, and back to 0 V again. No noticeable voltage hysteresis effects were observed.

At the operating wavelength of 1470 nm, the top gating voltage was observed to produce a slight increase in S_3, while the bottom gating voltage conversely reduced S_3. Together with the large changes in S_1 and S_2 from tuning the bottom gating voltage, this resulted in the two-parameter polarization control seen in Fig. 4.

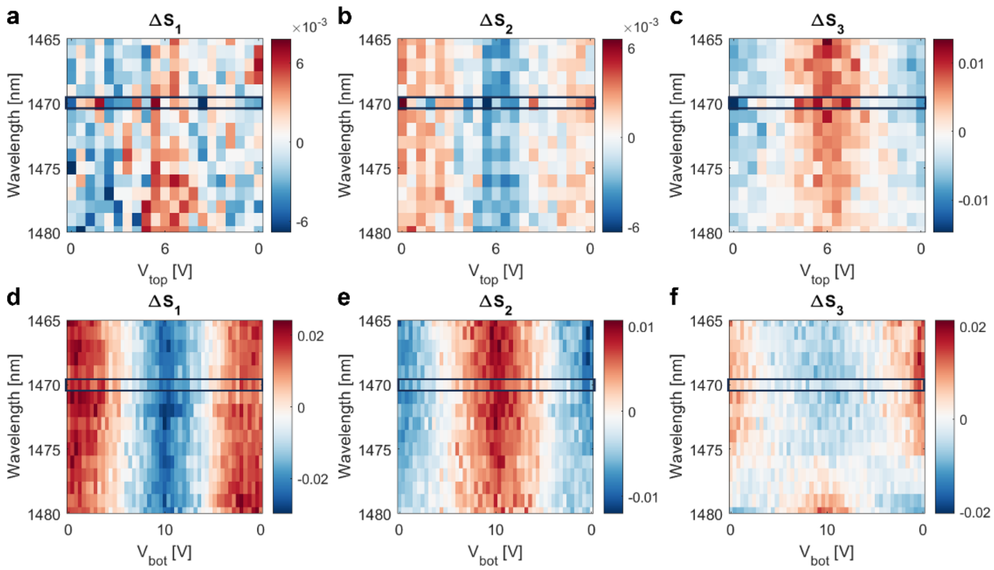

Supplementary Fig. 4. Mean-centered change of Stokes parameters as a function of wavelength and voltage. Voltages are swept from zero, to maximum, and back to zero again to probe hysteresis. The operating wavelength of 1470nm is highlighted with the blue rectangle. (a-c) Changes in Stokes parameters when varying BP-top voltage. S_1 and S_2 parameters experience minimal change, while S_3 increases slightly at maximum voltage. (d-f) Changes in Stokes parameters when varying BP-bottom voltage. S_1 and S_3 decreases, while S_2 increases slightly at maximum voltage. The reduction in S_3 when gating BP-bottom (as opposed to the increase in S_3 when gating BP-top) results in the two-parameter polarization control seen in Fig. 4.

Supplementary Note 5. Contrast microscopy for determining BP layer thickness

A background adjusted contrast measurement was done by comparing the average flake pixel intensity against the background immediately surrounding the flake. An average of 3.73% contrast per layer of BP was found to fit the data acquired by exfoliating 33 different samples of thin layer BP.

$$I_{contrast} = \frac{I_{flake} - I_{background}}{I_{flake} + I_{background}}$$

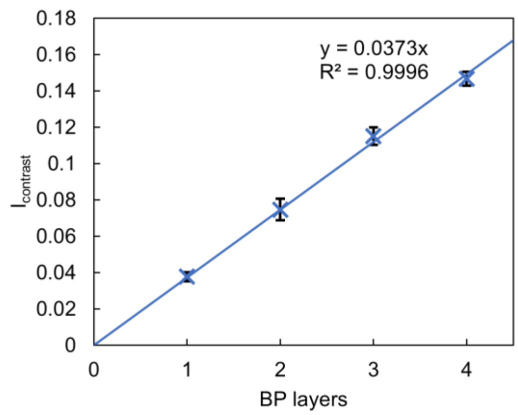

Supplementary Fig. 5. BP flake contrast measurements for determining BP layer thickness. Error bars show the standard deviation in contrast values across multiple exfoliated samples

Supplementary Note 6. Schematic for optical measurement setup

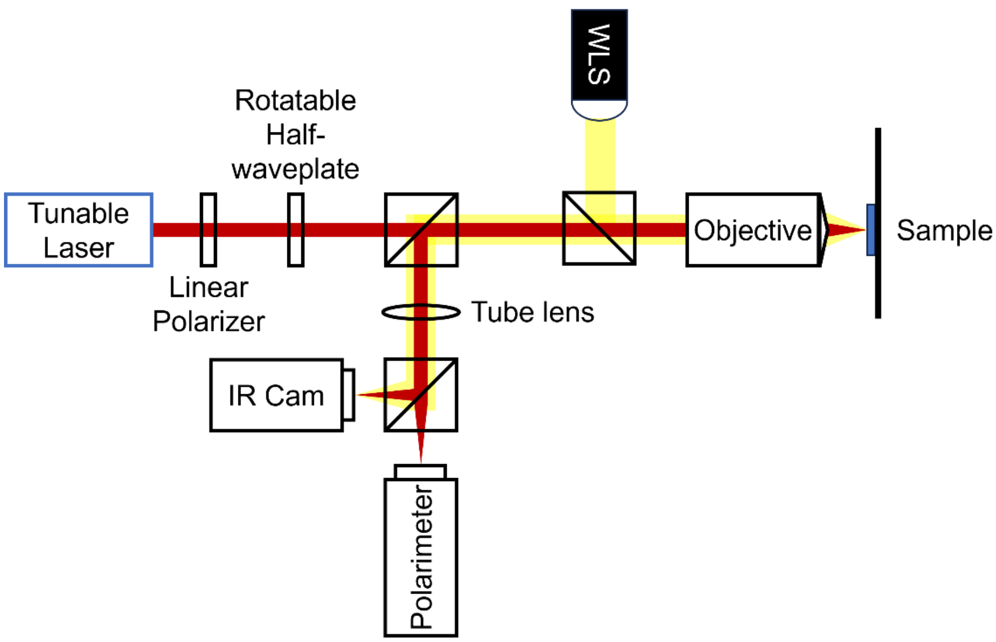

Supplementary Fig. 6. Schematic of the optical experimental setup. 'WLS' denotes the white light source that was used to image the device on the IR camera, which was turned off for polarimetry measurements.

Supplementary Note 7. Table of measurements for S-parameters as a function of two gating voltages

Tabulated data of S-parameters at each gating voltage, corresponding to data points in Fig. 4c.

V_{top} [V]	V_{bot} [V]	S_1	S_2	S_3
0	0.4	-0.19287	-0.90169	-0.38698
0.4	0.4	-0.19338	-0.90176	-0.38657
0.8	0.4	-0.19539	-0.90142	-0.38636
1.2	0.4	-0.19103	-0.90230	-0.38647
1.6	0.4	-0.19790	-0.90116	-0.38568

2	0.4	-0.19426	-0.90138	-0.38701
2.4	0.4	-0.19906	-0.90132	-0.38471
2.8	0.4	-0.19809	-0.90188	-0.38389
3.2	0.4	-0.19612	-0.90268	-0.38302
3.6	0.4	-0.19241	-0.90456	-0.38047
4	0.4	-0.19372	-0.90457	-0.37976
4.4	0.4	-0.19707	-0.90349	-0.38062
4.8	0.4	-0.19270	-0.90554	-0.37797
5.2	0.4	-0.19920	-0.90314	-0.38033
5.6	0.4	-0.19871	-0.90336	-0.38007
6	0.4	-0.20076	-0.90322	-0.37934
0	0.8	-0.19371	-0.90065	-0.38899
0.4	0.8	-0.19080	-0.90146	-0.38855
0.8	0.8	-0.19399	-0.90080	-0.38849
1.2	0.8	-0.18999	-0.90211	-0.38742
1.6	0.8	-0.19747	-0.90012	-0.38832
2	0.8	-0.19369	-0.90192	-0.38604
2.4	0.8	-0.19700	-0.90127	-0.38587
2.8	0.8	-0.19468	-0.90242	-0.38436
3.2	0.8	-0.19314	-0.90308	-0.38359
3.6	0.8	-0.19261	-0.90328	-0.38338
4	0.8	-0.19763	-0.90293	-0.38164
4.4	0.8	-0.19475	-0.90335	-0.38214
4.8	0.8	-0.19533	-0.90447	-0.37918
5.2	0.8	-0.19758	-0.90296	-0.38160
5.6	0.8	-0.20395	-0.90034	-0.38444
6	0.8	-0.20102	-0.90317	-0.37931
0	1.2	-0.19381	-0.90054	-0.38918
0.4	1.2	-0.19184	-0.90085	-0.38946
0.8	1.2	-0.19490	-0.90080	-0.38803
1.2	1.2	-0.19189	-0.90127	-0.38844
1.6	1.2	-0.19704	-0.90019	-0.38836
2	1.2	-0.19618	-0.90027	-0.38862
2.4	1.2	-0.19432	-0.90135	-0.38705
2.8	1.2	-0.19480	-0.90202	-0.38525
3.2	1.2	-0.19287	-0.90244	-0.38524
3.6	1.2	-0.19239	-0.90341	-0.38319
4	1.2	-0.19568	-0.90300	-0.38250
4.4	1.2	-0.19531	-0.90348	-0.38153
4.8	1.2	-0.19506	-0.90278	-0.38332
5.2	1.2	-0.20064	-0.90198	-0.38233
5.6	1.2	-0.20105	-0.90230	-0.38135
6	1.2	-0.20255	-0.89964	-0.38680
0	1.6	-0.19474	-0.89997	-0.39003
0.4	1.6	-0.19381	-0.90120	-0.38767
0.8	1.6	-0.19079	-0.90070	-0.39030
1.2	1.6	-0.19793	-0.89913	-0.39038
1.6	1.6	-0.19090	-0.90145	-0.38851
2	1.6	-0.19382	-0.90071	-0.38878
2.4	1.6	-0.19646	-0.90079	-0.38727
2.8	1.6	-0.19503	-0.90183	-0.38558
3.2	1.6	-0.18976	-0.90345	-0.38441
3.6	1.6	-0.19244	-0.90228	-0.38583
4	1.6	-0.19703	-0.90223	-0.38362
4.4	1.6	-0.19616	-0.90238	-0.38372
4.8	1.6	-0.19505	-0.90398	-0.38050
5.2	1.6	-0.20215	-0.90113	-0.38353
5.6	1.6	-0.19797	-0.90264	-0.38216
6	1.6	-0.19824	-0.90299	-0.38119
0	2	-0.19448	-0.89892	-0.39258
0.4	2	-0.19594	-0.89875	-0.39224
0.8	2	-0.19269	-0.89943	-0.39229

1.2	2	-0.19835	-0.89939	-0.38956
1.6	2	-0.19812	-0.89903	-0.39050
2	2	-0.19771	-0.89932	-0.39005
2.4	2	-0.20159	-0.89873	-0.38941
2.8	2	-0.19233	-0.90178	-0.38703
3.2	2	-0.19656	-0.90135	-0.38591
3.6	2	-0.19471	-0.90139	-0.38676
4	2	-0.19578	-0.90241	-0.38384
4.4	2	-0.19500	-0.90189	-0.38544
4.8	2	-0.19721	-0.90244	-0.38303
5.2	2	-0.19747	-0.90104	-0.38618
5.6	2	-0.19995	-0.90101	-0.38498
6	2	-0.19842	-0.90377	-0.37925
0	2.4	-0.19466	-0.89861	-0.39319
0.4	2.4	-0.19658	-0.89935	-0.39054
0.8	2.4	-0.19298	-0.90063	-0.38939
1.2	2.4	-0.19771	-0.89827	-0.39245
1.6	2.4	-0.19515	-0.89960	-0.39068
2	2.4	-0.19933	-0.89890	-0.39018
2.4	2.4	-0.19934	-0.89961	-0.38854
2.8	2.4	-0.19601	-0.90092	-0.38719
3.2	2.4	-0.19835	-0.90030	-0.38745
3.6	2.4	-0.19518	-0.90188	-0.38537
4	2.4	-0.19754	-0.90188	-0.38417
4.4	2.4	-0.19728	-0.90100	-0.38636
4.8	2.4	-0.19661	-0.90204	-0.38426
5.2	2.4	-0.20155	-0.90115	-0.38380
5.6	2.4	-0.20067	-0.90076	-0.38517
6	2.4	-0.20546	-0.89910	-0.38654
0	2.8	-0.19576	-0.89838	-0.39318
0.4	2.8	-0.20238	-0.89739	-0.39210
0.8	2.8	-0.19791	-0.89832	-0.39225
1.2	2.8	-0.20179	-0.89762	-0.39187
1.6	2.8	-0.19905	-0.89884	-0.39046
2	2.8	-0.19829	-0.89923	-0.38995
2.4	2.8	-0.19907	-0.89962	-0.38867
2.8	2.8	-0.19789	-0.89938	-0.38982
3.2	2.8	-0.20114	-0.89934	-0.38824
3.6	2.8	-0.19768	-0.90060	-0.38710
4	2.8	-0.19872	-0.90018	-0.38753
4.4	2.8	-0.19887	-0.90045	-0.38683
4.8	2.8	-0.19732	-0.90175	-0.38460
5.2	2.8	-0.20561	-0.89972	-0.38500
5.6	2.8	-0.20449	-0.89991	-0.38516
6	2.8	-0.20489	-0.90067	-0.38315
0	3.2	-0.19923	-0.89778	-0.39282
0.4	3.2	-0.20248	-0.89797	-0.39070
0.8	3.2	-0.20000	-0.89792	-0.39210
1.2	3.2	-0.20107	-0.89808	-0.39117
1.6	3.2	-0.19911	-0.89832	-0.39163
2	3.2	-0.19863	-0.89865	-0.39112
2.4	3.2	-0.20200	-0.89854	-0.38964
2.8	3.2	-0.20467	-0.89788	-0.38978
3.2	3.2	-0.19824	-0.89995	-0.38832
3.6	3.2	-0.20085	-0.89897	-0.38925
4	3.2	-0.19800	-0.90065	-0.38683
4.4	3.2	-0.20114	-0.90052	-0.38550
4.8	3.2	-0.20226	-0.89955	-0.38717
5.2	3.2	-0.20623	-0.89787	-0.38897
5.6	3.2	-0.20661	-0.89787	-0.38878
6	3.2	-0.20653	-0.90029	-0.38318
0	3.6	-0.20318	-0.89695	-0.39268

0.4	3.6	-0.20270	-0.89684	-0.39319
0.8	3.6	-0.20254	-0.89692	-0.39308
1.2	3.6	-0.20325	-0.89692	-0.39272
1.6	3.6	-0.20004	-0.89796	-0.39199
2	3.6	-0.20097	-0.89818	-0.39101
2.4	3.6	-0.20856	-0.89652	-0.39084
2.8	3.6	-0.20507	-0.89781	-0.38973
3.2	3.6	-0.20012	-0.89900	-0.38955
3.6	3.6	-0.19994	-0.89980	-0.38780
4	3.6	-0.20209	-0.89962	-0.38710
4.4	3.6	-0.20183	-0.89914	-0.38834
4.8	3.6	-0.20336	-0.90007	-0.38538
5.2	3.6	-0.20416	-0.89932	-0.38671
5.6	3.6	-0.20476	-0.89978	-0.38531
6	3.6	-0.20211	-0.89883	-0.38892
0	4	-0.20461	-0.89527	-0.39575
0.4	4	-0.20429	-0.89573	-0.39488
0.8	4	-0.20288	-0.89676	-0.39327
1.2	4	-0.20516	-0.89652	-0.39264
1.6	4	-0.20589	-0.89645	-0.39240
2	4	-0.20044	-0.89909	-0.38917
2.4	4	-0.20763	-0.89629	-0.39187
2.8	4	-0.20447	-0.89753	-0.39068
3.2	4	-0.20330	-0.89809	-0.39001
3.6	4	-0.20462	-0.89870	-0.38790
4	4	-0.20577	-0.89949	-0.38546
4.4	4	-0.20892	-0.89714	-0.38922
4.8	4	-0.20448	-0.89926	-0.38667
5.2	4	-0.20702	-0.89769	-0.38898
5.6	4	-0.20435	-0.89848	-0.38855
6	4	-0.20682	-0.89659	-0.39160
0	4.4	-0.20613	-0.89559	-0.39424
0.4	4.4	-0.20835	-0.89497	-0.39450
0.8	4.4	-0.20659	-0.89592	-0.39325
1.2	4.4	-0.20794	-0.89549	-0.39352
1.6	4.4	-0.20664	-0.89651	-0.39187
2	4.4	-0.20666	-0.89558	-0.39400
2.4	4.4	-0.20473	-0.89686	-0.39208
2.8	4.4	-0.20981	-0.89634	-0.39057
3.2	4.4	-0.20570	-0.89822	-0.38844
3.6	4.4	-0.20303	-0.89905	-0.38792
4	4.4	-0.20985	-0.89808	-0.38653
4.4	4.4	-0.20882	-0.89747	-0.38852
4.8	4.4	-0.20747	-0.89770	-0.38871
5.2	4.4	-0.20838	-0.89813	-0.38723
5.6	4.4	-0.20781	-0.89627	-0.39180
6	4.4	-0.20619	-0.89937	-0.38551
0	4.8	-0.20921	-0.89440	-0.39532
0.4	4.8	-0.20540	-0.89532	-0.39524
0.8	4.8	-0.20865	-0.89497	-0.39432
1.2	4.8	-0.20911	-0.89469	-0.39471
1.6	4.8	-0.20797	-0.89580	-0.39280
2	4.8	-0.20726	-0.89631	-0.39202
2.4	4.8	-0.20655	-0.89673	-0.39141
2.8	4.8	-0.20791	-0.89703	-0.39000
3.2	4.8	-0.20894	-0.89717	-0.38914
3.6	4.8	-0.20651	-0.89760	-0.38945
4	4.8	-0.21123	-0.89644	-0.38959
4.4	4.8	-0.21104	-0.89654	-0.38946
4.8	4.8	-0.21238	-0.89558	-0.39094
5.2	4.8	-0.21164	-0.89555	-0.39141
5.6	4.8	-0.21035	-0.89687	-0.38908

6	4.8	-0.21482	-0.89560	-0.38956
0	5.2	-0.21086	-0.89507	-0.39292
0.4	5.2	-0.20921	-0.89462	-0.39483
0.8	5.2	-0.21022	-0.89496	-0.39352
1.2	5.2	-0.21213	-0.89444	-0.39366
1.6	5.2	-0.20886	-0.89511	-0.39389
2	5.2	-0.21100	-0.89508	-0.39283
2.4	5.2	-0.20710	-0.89690	-0.39075
2.8	5.2	-0.21215	-0.89564	-0.39092
3.2	5.2	-0.21535	-0.89571	-0.38900
3.6	5.2	-0.20985	-0.89695	-0.38916
4	5.2	-0.21216	-0.89673	-0.38842
4.4	5.2	-0.21385	-0.89620	-0.38870
4.8	5.2	-0.21306	-0.89551	-0.39073
5.2	5.2	-0.21220	-0.89480	-0.39282
5.6	5.2	-0.21375	-0.89690	-0.38714
6	5.2	-0.21539	-0.89497	-0.39068
0	5.6	-0.21568	-0.89303	-0.39494
0.4	5.6	-0.21048	-0.89465	-0.39408
0.8	5.6	-0.20793	-0.89530	-0.39396
1.2	5.6	-0.21200	-0.89500	-0.39246
1.6	5.6	-0.20994	-0.89498	-0.39363
2	5.6	-0.21451	-0.89445	-0.39235
2.4	5.6	-0.21335	-0.89478	-0.39223
2.8	5.6	-0.21425	-0.89407	-0.39336
3.2	5.6	-0.21471	-0.89478	-0.39149
3.6	5.6	-0.21199	-0.89584	-0.39056
4	5.6	-0.21504	-0.89647	-0.38743
4.4	5.6	-0.21370	-0.89545	-0.39050
4.8	5.6	-0.21449	-0.89601	-0.38879
5.2	5.6	-0.21454	-0.89463	-0.39192
5.6	5.6	-0.21394	-0.89555	-0.39015
6	5.6	-0.21499	-0.89705	-0.38610
0	6	-0.21160	-0.89306	-0.39708
0.4	6	-0.21124	-0.89401	-0.39511
0.8	6	-0.21337	-0.89338	-0.39540
1.2	6	-0.21589	-0.89308	-0.39472
1.6	6	-0.21223	-0.89409	-0.39442
2	6	-0.21414	-0.89418	-0.39318
2.4	6	-0.21792	-0.89358	-0.39246
2.8	6	-0.21483	-0.89400	-0.39322
3.2	6	-0.21528	-0.89491	-0.39087
3.6	6	-0.21225	-0.89660	-0.38866
4	6	-0.21430	-0.89552	-0.39002
4.4	6	-0.21610	-0.89499	-0.39025
4.8	6	-0.21734	-0.89395	-0.39193
5.2	6	-0.21492	-0.89707	-0.38609
5.6	6	-0.21816	-0.89293	-0.39381
6	6	-0.21776	-0.89328	-0.39323
0	6.4	-0.21536	-0.89179	-0.39791
0.4	6.4	-0.21134	-0.89379	-0.39558
0.8	6.4	-0.21690	-0.89226	-0.39603
1.2	6.4	-0.21599	-0.89293	-0.39500
1.6	6.4	-0.21614	-0.89288	-0.39504
2	6.4	-0.21501	-0.89439	-0.39223
2.4	6.4	-0.21696	-0.89390	-0.39226
2.8	6.4	-0.21437	-0.89422	-0.39295
3.2	6.4	-0.21707	-0.89467	-0.39044
3.6	6.4	-0.21420	-0.89598	-0.38903
4	6.4	-0.21808	-0.89456	-0.39014
4.4	6.4	-0.21787	-0.89466	-0.39003
4.8	6.4	-0.21818	-0.89392	-0.39155

5.2	6.4	-0.21749	-0.89398	-0.39178
5.6	6.4	-0.21909	-0.89364	-0.39167
6	6.4	-0.21729	-0.89570	-0.38795
0	6.8	-0.21714	-0.89140	-0.39781
0.4	6.8	-0.21658	-0.89152	-0.39786
0.8	6.8	-0.21614	-0.89212	-0.39675
1.2	6.8	-0.21663	-0.89232	-0.39602
1.6	6.8	-0.21441	-0.89397	-0.39351
2	6.8	-0.21891	-0.89239	-0.39462
2.4	6.8	-0.21908	-0.89305	-0.39301
2.8	6.8	-0.21740	-0.89414	-0.39146
3.2	6.8	-0.21764	-0.89430	-0.39097
3.6	6.8	-0.21520	-0.89507	-0.39056
4	6.8	-0.21924	-0.89372	-0.39140
4.4	6.8	-0.21689	-0.89490	-0.39002
4.8	6.8	-0.22010	-0.89382	-0.39069
5.2	6.8	-0.22398	-0.89275	-0.39093
5.6	6.8	-0.21745	-0.89510	-0.38924
6	6.8	-0.22317	-0.89350	-0.38968
0	7.2	-0.21920	-0.89124	-0.39704
0.4	7.2	-0.21732	-0.89154	-0.39741
0.8	7.2	-0.21629	-0.89202	-0.39689
1.2	7.2	-0.21976	-0.89198	-0.39507
1.6	7.2	-0.21992	-0.89141	-0.39627
2	7.2	-0.22227	-0.89137	-0.39503
2.4	7.2	-0.21975	-0.89222	-0.39453
2.8	7.2	-0.21845	-0.89299	-0.39352
3.2	7.2	-0.21891	-0.89408	-0.39078
3.6	7.2	-0.21862	-0.89372	-0.39175
4	7.2	-0.21929	-0.89425	-0.39015
4.4	7.2	-0.22182	-0.89292	-0.39178
4.8	7.2	-0.22027	-0.89445	-0.38915
5.2	7.2	-0.22521	-0.89108	-0.39404
5.6	7.2	-0.22042	-0.89308	-0.39220
6	7.2	-0.22543	-0.89341	-0.38859
0	7.6	-0.22577	-0.88911	-0.39814
0.4	7.6	-0.22477	-0.88921	-0.39847
0.8	7.6	-0.22325	-0.89057	-0.39630
1.2	7.6	-0.22468	-0.89095	-0.39463
1.6	7.6	-0.22664	-0.88925	-0.39732
2	7.6	-0.22706	-0.89040	-0.39449
2.4	7.6	-0.22460	-0.89049	-0.39570
2.8	7.6	-0.22623	-0.89071	-0.39428
3.2	7.6	-0.22637	-0.89159	-0.39220
3.6	7.6	-0.21851	-0.89418	-0.39077
4	7.6	-0.22250	-0.89304	-0.39112
4.4	7.6	-0.22382	-0.89217	-0.39235
4.8	7.6	-0.22784	-0.89138	-0.39183
5.2	7.6	-0.22672	-0.89135	-0.39255
5.6	7.6	-0.22499	-0.89247	-0.39100
6	7.6	-0.22678	-0.89019	-0.39513
0	8	-0.22688	-0.88913	-0.39746
0.4	8	-0.22880	-0.88767	-0.39962
0.8	8	-0.22176	-0.89072	-0.39679
1.2	8	-0.22383	-0.89013	-0.39694
1.6	8	-0.22613	-0.88973	-0.39655
2	8	-0.22427	-0.89045	-0.39598
2.4	8	-0.22334	-0.89116	-0.39490
2.8	8	-0.22444	-0.89133	-0.39390
3.2	8	-0.22334	-0.89245	-0.39199
3.6	8	-0.22266	-0.89235	-0.39261
4	8	-0.22492	-0.89227	-0.39150

4.4	8	-0.22539	-0.89152	-0.39291
4.8	8	-0.22387	-0.89191	-0.39292
5.2	8	-0.22671	-0.89030	-0.39493
5.6	8	-0.22703	-0.89097	-0.39324
6	8	-0.22658	-0.89218	-0.39073
0	8.4	-0.22364	-0.89048	-0.39628
0.4	8.4	-0.22760	-0.88884	-0.39769
0.8	8.4	-0.22332	-0.89046	-0.39650
1.2	8.4	-0.22511	-0.89004	-0.39642
1.6	8.4	-0.22701	-0.88948	-0.39661
2	8.4	-0.23084	-0.88882	-0.39587
2.4	8.4	-0.22655	-0.89038	-0.39483
2.8	8.4	-0.22815	-0.89064	-0.39333
3.2	8.4	-0.22575	-0.89111	-0.39365
3.6	8.4	-0.22863	-0.89086	-0.39255
4	8.4	-0.22807	-0.89086	-0.39287
4.4	8.4	-0.22733	-0.89187	-0.39100
4.8	8.4	-0.22883	-0.89075	-0.39269
5.2	8.4	-0.23251	-0.88825	-0.39618
5.6	8.4	-0.23203	-0.89060	-0.39114
6	8.4	-0.22993	-0.88954	-0.39477
0	8.8	-0.23332	-0.88686	-0.39881
0.4	8.8	-0.23356	-0.88735	-0.39757
0.8	8.8	-0.22630	-0.88972	-0.39647
1.2	8.8	-0.22862	-0.88858	-0.39769
1.6	8.8	-0.23061	-0.88837	-0.39702
2	8.8	-0.23546	-0.88651	-0.39831
2.4	8.8	-0.23200	-0.88934	-0.39402
2.8	8.8	-0.22911	-0.88998	-0.39427
3.2	8.8	-0.23067	-0.89015	-0.39296
3.6	8.8	-0.22941	-0.89114	-0.39147
4	8.8	-0.22814	-0.89145	-0.39149
4.4	8.8	-0.23342	-0.89044	-0.39069
4.8	8.8	-0.23101	-0.88980	-0.39355
5.2	8.8	-0.23346	-0.88948	-0.39285
5.6	8.8	-0.23562	-0.88725	-0.39658
6	8.8	-0.22887	-0.89138	-0.39123
0	9.2	-0.23585	-0.88508	-0.40126
0.4	9.2	-0.23039	-0.88820	-0.39753
0.8	9.2	-0.22822	-0.88928	-0.39634
1.2	9.2	-0.23063	-0.88839	-0.39696
1.6	9.2	-0.23265	-0.88795	-0.39676
2	9.2	-0.22992	-0.88889	-0.39625
2.4	9.2	-0.23117	-0.88928	-0.39464
2.8	9.2	-0.23479	-0.88820	-0.39493
3.2	9.2	-0.23352	-0.88897	-0.39395
3.6	9.2	-0.23380	-0.88946	-0.39268
4	9.2	-0.23196	-0.89006	-0.39242
4.4	9.2	-0.23676	-0.88890	-0.39218
4.8	9.2	-0.23422	-0.88845	-0.39472
5.2	9.2	-0.23312	-0.89007	-0.39171
5.6	9.2	-0.23616	-0.88855	-0.39333
6	9.2	-0.23254	-0.89105	-0.38981
0	9.6	-0.23562	-0.88557	-0.40030
0.4	9.6	-0.23292	-0.88744	-0.39774
0.8	9.6	-0.23411	-0.88736	-0.39723
1.2	9.6	-0.23230	-0.88715	-0.39874
1.6	9.6	-0.23620	-0.88639	-0.39815
2	9.6	-0.23267	-0.88869	-0.39510
2.4	9.6	-0.23606	-0.88752	-0.39571
2.8	9.6	-0.23065	-0.88972	-0.39395
3.2	9.6	-0.23785	-0.88729	-0.39515

3.6	9.6	-0.23215	-0.88942	-0.39376
4	9.6	-0.23430	-0.88930	-0.39274
4.4	9.6	-0.23275	-0.89035	-0.39129
4.8	9.6	-0.23564	-0.88906	-0.39248
5.2	9.6	-0.24039	-0.88729	-0.39361
5.6	9.6	-0.23154	-0.88973	-0.39342
6	9.6	-0.23316	-0.89039	-0.39095
0	10	-0.23412	-0.88613	-0.39995
0.4	10	-0.23498	-0.88600	-0.39973
0.8	10	-0.23796	-0.88599	-0.39798
1.2	10	-0.23812	-0.88608	-0.39769
1.6	10	-0.23482	-0.88688	-0.39788
2	10	-0.23514	-0.88777	-0.39570
2.4	10	-0.23932	-0.88709	-0.39470
2.8	10	-0.23433	-0.88876	-0.39396
3.2	10	-0.23837	-0.88775	-0.39379
3.6	10	-0.23675	-0.88823	-0.39369
4	10	-0.23428	-0.88906	-0.39331
4.4	10	-0.23379	-0.88933	-0.39298
4.8	10	-0.23950	-0.88767	-0.39330
5.2	10	-0.24020	-0.88705	-0.39426
5.6	10	-0.23903	-0.88676	-0.39562
6	10	-0.24233	-0.88677	-0.39360

Supplementary Note 8. Effect of input polarization angle on Poincare sphere coverage

In the critically coupled case, rotating the input polarization angle away from the AC axis of one of the BP layers reduces the tunability of the electric field along that direction. This results in a vertical or horizontal stretching of the S_0, ψ and χ voltage maps in Fig. 2c-e. For example, a 15° input relative to the bottom BP layer's AC-axis horizontally elongates the critically coupled point as the reflected light becomes less sensitive to modulations of the top BP layer (Supplementary Fig. 8a-c). This elongation also decreases the average optical efficiency of the device (Supplementary Fig. 8g), while decreasing the overall Poincare sphere coverage (Supplementary Fig. 8h). We note that the sharp drop off seen in Supplementary Fig. 8h occurs when significant features of the azimuthal and elliptical maps are cut off due to the large horizontal stretching at lower input angles. However, the coverage is relatively agnostic to input polarization in the 20-45° input range as the ellipse parameter singularity features are still largely accessible within the voltage parameter space.

Similar trends were observed in the non-critically coupled case, where the top PMMA layer thickness was reduced from the optimal 490 nm to 470 nm, causing the critically coupled point to be inaccessible through gating. However, in this case since the optical phase singularity is no longer accessible, horizontal stretching of the plot linearly reduces the polarization coverage instead (Supplementary Fig. 8i).

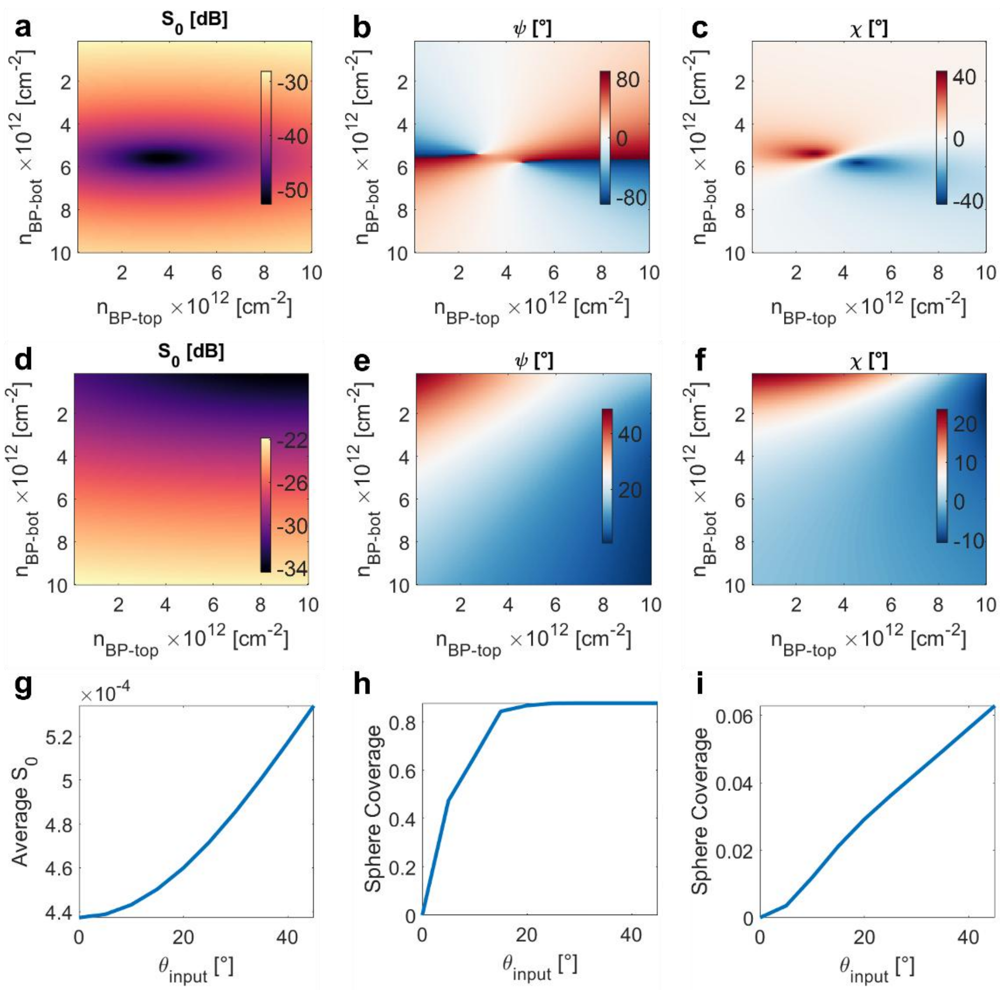

Supplementary Fig. 8. Effect of input polarization angle on polarization modulation. (**a-c**) S_0, azimuthal and elliptical maps as a function of top and bottom carrier densities, for the same device presented in Fig. 1 & 2, but with a 15° input polarization angle to the bottom BP flake's AC axis. (**d-f**) S_0, azimuthal and elliptical maps as a function of top and bottom carrier densities, for a non-critically coupled case where the top PMMA layer is reduced from the optimal 490 nm to 470 nm, and with a 15° input angle. (**g**) and (**h**) are the average S_0 and the total Poincare sphere coverage as a function of input polarization angle for the critically coupled case (a-c), while (**i**) shows the Poincare sphere coverage for the non-critically coupled case (d-f).

Supplementary Note 9. Results for second dual-gated BP polarization control device

To explicitly show reproducibility of the results for our device design, we fabricated an additional device, with the results summarized in Supplementary Fig. 9. The micrograph of the device is shown in Supplementary Fig. 9a, together with the Raman measurement results of the BP flakes and the input polarization angle (55° to the horizontal). The passive spectral polarization tuning is summarized in Supplementary Fig. 9b, showing a reflectance minima of 1.5% due to a more accurate thickness of gold being deposited. Two-parameter polarization control is demonstrated with the new device, showing dependence of both ellipse parameters on both the top and bottom gating voltages (Supplementary Fig. 9c-e).

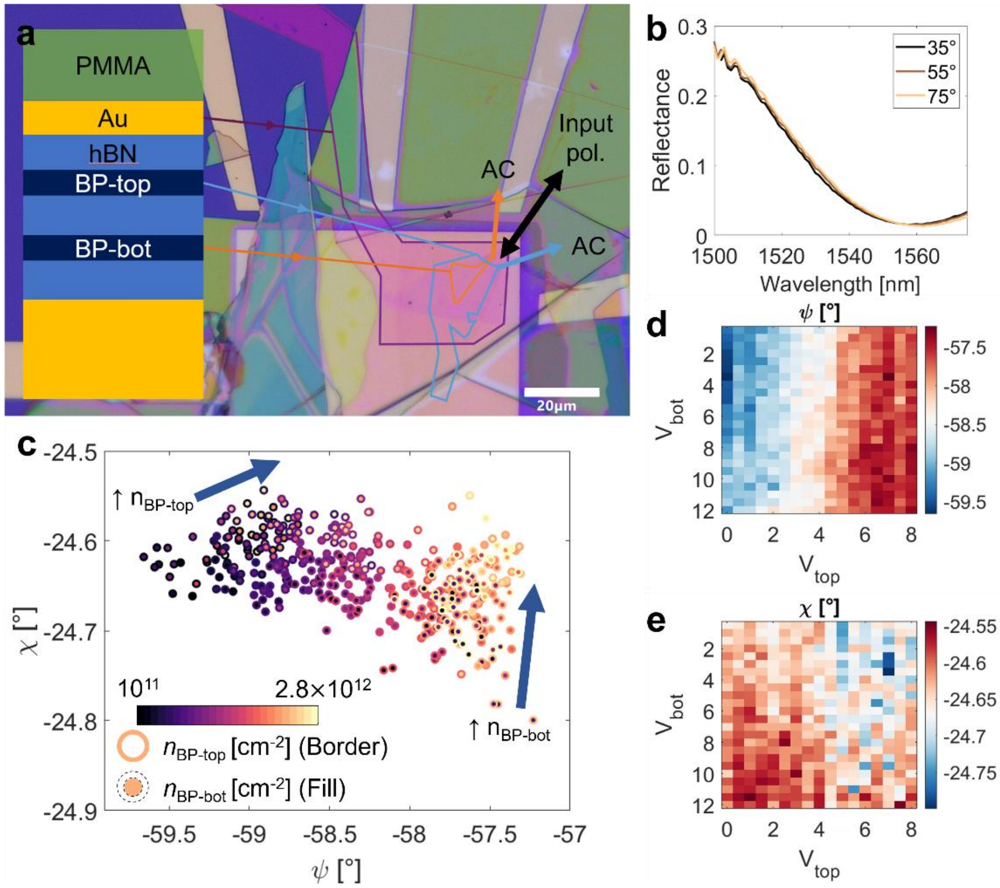

Supplementary Fig. 9. Fabrication and experimental results of the second dual-gated BP device. (**a**) Optical image of the device, with the top gold mirror, top BP layer and bottom BP layer outlined in purple, blue and orange respectively. Inset shows the cross-sectional schematic. The top BP layer makes electrical contact with the north-eastern gold finger, while the bottom BP layer is contacted by the eastern gold finger. The AC axis separation of the two BP layers was determined to be 66°. The black double headed arrow marks the input polarization angle of 55° used in subsequent measurements. White scale bar represents 20 μm. (**b**) Normalized reflectance of the device at different input polarization angles, showing a 1.5% minimum at 1561 nm. (**c**) Normalized Poincare sphere plot showing 2D polarization coverage over Poincare sphere. The top (bottom) BP doping density is represented in border (fill) color of the plot points (from black to peach). (**d** and **e**) Measured azimuthal and elliptical coordinate as a function of top and bottom gating.

Overall, the device, while being marginally better coupled, has a smaller active area (owing to a smaller 3L-BP bottom flake), is more detuned away from the exciton resonance wavelength (due to a thicker cavity), has poorer AC-axes alignment (66° separation), and has a smaller spectral overlap between the top and bottom BP flakes (due to imperfect top and bottom hBN flake thicknesses). This resulted in a Poincare sphere coverage that was about 60% less than the original device in Fig. 3-5.

Nonetheless, we note that none of the above factors fundamentally precludes the possibility of a device spanning a larger polarization coverage range. Using cleaner pickup and transfer techniques[1], performing Raman microscopy within the glovebox to determine BP crystallographic direction before stacking, more precise and judicious selection for hBN flake thickness, careful seeding of the top gold layer to minimize mirror roughness, and exfoliating larger 3L-BP flakes than those used in this work are but some ways in which device fabrication could be improved. Here, we propose and demonstrate a new way of electronic polarization modulation via two-parameter control. While an optimal device fabrication remains difficult owing to its sensitivity to many different factors (top gold thickness, size and quality of flakes, alignment of BP flakes, thickness of each of the 5-layers, cleanliness of sample), we show proof of concept of this 2D control with varying degrees of polarization coverage.

Supplementary Note 10. Poincare sphere coverage as a function of intracavity loss

In Fig. 5c, intracavity losses were introduced into the model to account for heterostructure imperfections and match the transfer matrix model to the experimental reflectance results. These additional losses, modelled as a distributed loss through the cavity by increasing the imaginary refractive index of the hBN dielectric, effectively reduce the Q of the device. This firstly leads to reduced phase buildup within the cavity. Secondly, the increased reflectance linewidth results in a reduction in anisotropic amplitude ratio modulation under gating. Combined, the reduced device Q therefore causes the total Poincare sphere coverage to drop (Supplementary Fig. 10).

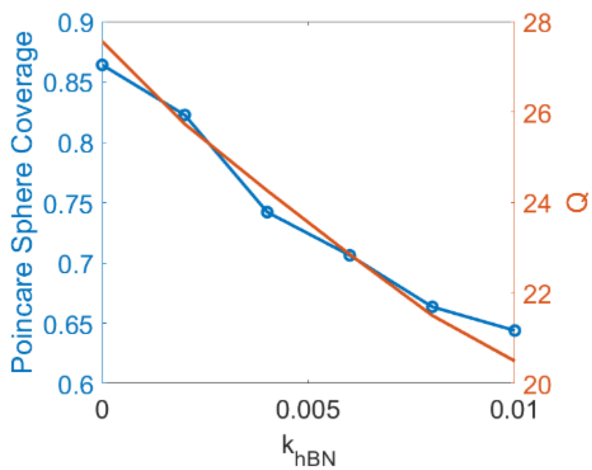

Supplementary Fig. 10. Simulated Poincare sphere coverage and cavity Q as a function of intracavity loss (modelled by increasing the imaginary part of the hBN dielectric). The reduction in Q reduces the anisotropic amplitude ratio modulation and phase modulation of the device, which causes total coverage to drop

Supplementary Note 11. Possible sources of error for experimental vs simulation discrepancy in Fig. 5b

Firstly, we note the sensitivity of the device to the thickness of the top gold layer. Supplementary Fig. 11 shows the simulated Poincare sphere coverage for the device in Fig. 1, as a function of gold thickness. As the polarization modulation is maximized at critical coupling, the coverage is significantly affected by gold thickness at the angstrom level, with coverage dropping below 5% for gold that is >1 nm off in thickness. In practice, it is difficult to achieve angstrom-accurate gold deposition, especially without knowing the intracavity heterostructure losses a priori. The AFM measurement of the deposited gold (which is fed into the simulations) also has a sensitivity limit of a few angstroms, possibly explaining the discrepancy in Fig. 5b.

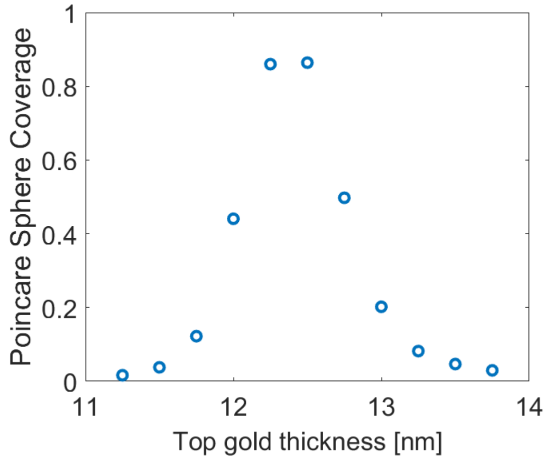

Supplementary Fig. 11. Simulated Poincare sphere coverage as a function of top gold thickness for the device in Fig. 1 and 2, showing optimal coverage at a thickness of ≈12.5 nm. 1 nm away from the optimal thickness, the coverage drops below 5%.

The sensitivity of the device to the top gold layer also underpins the importance on the gold deposition quality. At these small thicknesses, evaporator conditions heavily influence the crystallinity of the deposited gold. There is a need to properly seed the gold layer to avoid island-like growth as seen in reference [2]. For our fabrication, the gold layer was seeded with 1 nm of Ti, but no optimization studies were done to determine the dependence of gold roughness on the seeding layer for a hBN substrate. We recognize this as a potential subject for further studies to improve the overall Poincare sphere coverage.

Other possible reasons for the discrepancy relate to the simple capacitance model for estimating carrier concentrations and exciton oscillator strength as a function of gating voltage. The model neglects effects such as inefficiencies in the gold contacts and interconnects due to resistance, and the quantum capacitance of the BP layer.[3,4] Furthermore, defects within the BP layers are expected to locally trap excitons[5], while exciton-phonon interactions can limit exciton mobility.[6] These effects could potentially reduce the exciton oscillator strength dependence on carrier density.

Supplementary Note 12. Complex amplitude/360° phase modulation with a 2D heterostructure

To illustrate the 2D-parameter control result beyond polarization tuning, we show an additional example below where we cover the phase/amplitude parameter space by replacing one of the 3L-BP layers with graphene (Supplementary Fig. 12). Here, the graphene refractive index model as a function of doping is extensively described in reference [7]. Since each of the active 2D materials have differing refractive index responses to doping, and their relative placements within the cavity result in differing interactions with the electric field, their respective 1D gating trajectories on the complex reflection plane are inherently different. Combined, this allows for a 2D patch to be accessible via the multiplication of their respective 1D trajectories, which in turn allows the coefficients around the origin to be accessible, implying fully independent amplitude and 360° phase control. Previous similar work on complex modulation was demonstrated by employing a thick layer of indium tin oxide that could build differing charge carrier densities along its top and bottom interfaces.[8] The work presented in the manuscript provides evidence for the experimental viability of two-parameter control via atomically thin heterostructures instead.

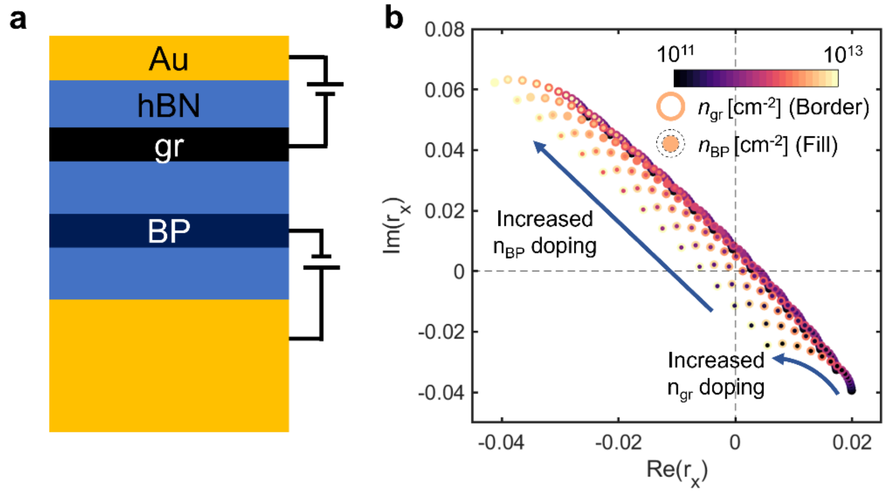

Supplementary Fig. 12. Full independent amplitude and 360° phase modulation device design and simulation. (**a**) Schematic of device. A sheet of p-doped (0.4eV) graphene (gr) is gated against the top gold contact, while a 3L-BP sheet is gated against the gold back reflector. Linearly polarized light is launched parallel to the AC-axis of the BP layer. (**b**) Simulated complex reflectivity plot of the device at 1502 nm, as a function of carrier densities in the graphene and 3L-BP. Independent control of the carrier densities generates reflection coefficients that pass through and around the origin, indicating independent 360° phase modulation and amplitude modulation.

Supplementary Note 13. Variation of polarization modulation with working wavelength

While the fabricated device would have a maximum Poincare sphere coverage at the reflectance minimum at 1470 nm, polarization modulation was still observed at 1481 nm (Supplementary Fig. 13a, b). We note that the coverage at 1481 nm is approximately 25% less than at 1470 nm due to the reduction in coupling. Furthermore, we note that the top BP sheet (which primarily controls the output azimuth angle) is better coupled at higher wavelengths. Conversely, the bottom BP sheet is better coupled at lower wavelengths (as seen in Fig. 4a). This indicates imperfect spectral overlap of the E_x and E_y resonances, which can be fixed by carefully adjusting the thickness of the topmost and bottommost hBN sheets to give equal electric field interaction to both the top and bottom BP sheets.

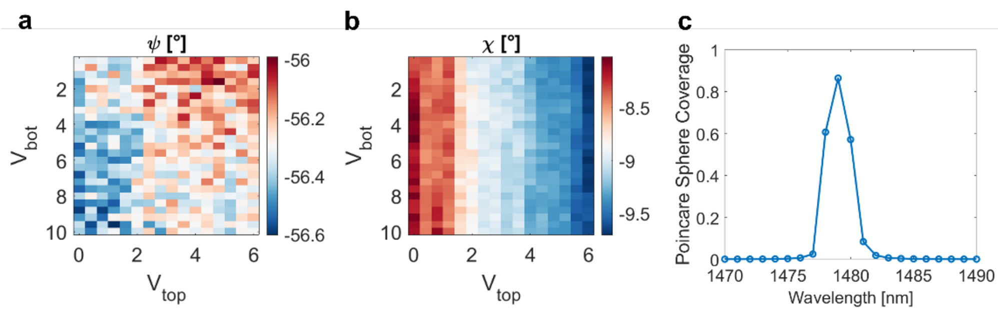

Supplementary Fig. 13. Effect of working wavelength on polarization modulation. (**a** and **b**) Measured azimuthal and elliptical coordinate as a function of top and bottom gating at an operating wavelength of 1481nm. Total polarization coverage here is about 25% less compared to Fig. 4a, b, due to the decreased coupling from operating at the off-resonance wavelength. (**c**) Poincare sphere coverage as a function of working wavelength for the critically coupled case shown in Fig. 1. At the critically coupled regime, the narrow linewidth of the resonance results in a narrow range of operating wavelengths.

For the ideal critically coupled case, the Poincare sphere coverage falls off more sharply than in the experimental under-coupled case (Supplementary Fig. 13c). By comparing against Fig. 2a, b, we see that phase modulation falls off sharply away from the operating wavelength (black dotted line in Fig. 2a, b), and that the amplitude ratio modulation also falls off when moving away from the E_x and E_y minima. This is in agreement with the sharp peak seen in Supplementary Fig. 13c.

We note that the Poincare sphere coverage maximum can be replicated at different wavelengths by modifying the thickness of the hBN dielectric and therefore the Fabry-Perot cavity resonance. The main limiting factor for operating wavelength is the exciton resonance, where modulation drops steadily at sufficiently detuned wavelengths. This is experimentally shown at 1562 nm in supplementary note 9 where a device with a different cavity thickness was made. However, even ~160 nm away from exciton resonance, sufficient spectral overlap between the exciton and cavity exists to measure polarization modulation.

Supplementary Note 14. Absolute reflectance and normalization plots

Reflectance plots in Fig. 3c were normalized against PMMA (460 nm) on gold (110 nm). The absolute reflectance measurements for the device, PMMA-covered gold reference, and the dark spectrum (taken with a beam block between objective and beam splitters) are plotted in Supplementary Fig. 14a for the 17° plot in Fig. 3c. Less than 0.01% reflectance variation is expected across the spectral measurement window for the PMMA-on-gold reference, as shown by transfer matrix calculations (Supplementary Fig. 14b).

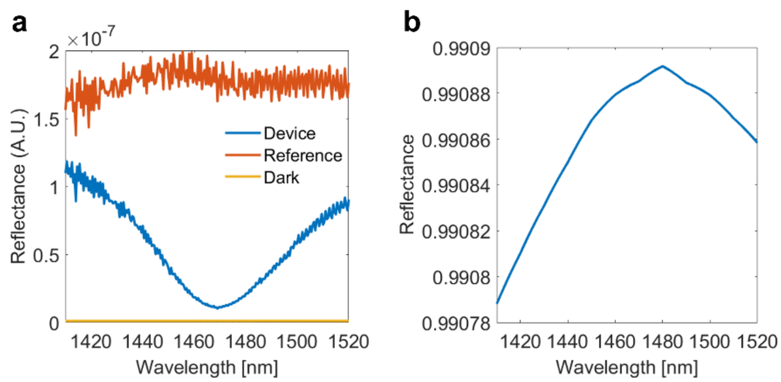

Supplementary Fig. 14. (**a**) Absolute reflectance measurements for the 17° plot in Fig. 3c, showing the device, PMMA-covered gold reference, and dark reflectances. (**b**) Transfer matrix model calculated reflectance of 460 nm PMMA on 110 nm gold.

Supplementary Note 15. Effect of objective lens on input polarization state to the device

While the objective lens does introduce some electric field energy into the longitudinal fields, the effect is expected to be small for our optical setup parameters. This can be explicitly evaluated using equation (3.66) in reference [9]. Here, we use NA = 0.4, and a moderate filling factor of $f_0 = 1$. By numerically solving the integrals for the electric field of the (0,0) mode, we find that for our objective, if linearly polarized light is launched along the E_x-direction, then:

$$\frac{Max(E_y^2)}{Max(E_x^2)} = 6 \times 10^{-5}, \frac{Max(E_z^2)}{Max(E_x^2)} = 0.017$$

The amount of energy in the y-direction is significantly less than the precision error of tuning the rotatable half-waveplate that determines the input polarization angle into the device, indicating that focusing has a negligible effect on the in-plane polarization angle. The energy in E_z from focusing is expected to slightly smear out the reflectance spectra due to having a very narrow range of incident angles into the Fabry-Perot cavity. This may explain the slightly broader linewidth of the black curve in Fig. 5a compared to the simulated orange curve (which assumes purely plane-wave incident light). Nonetheless, at 1.7% energy in E_z compared to E_x, and at a NA of 0.4, this effect is expected to be significantly less than the discrepancies observed between the black (experiment) and dotted red curve (lossless cavity simulation) in Fig. 5a.

Supplementary Note 16. Degree of depolarization in measurements

In Fig. 4c, the average degree of polarization across the data was measured to be:

$$Mean\left(\frac{P_{pol}}{P_{pol}+P_{unpol}}\right) = 88.4\%$$

There are several sources expected to contribute to this. Firstly, the objective lens, the beam splitter and the tube lens in the setup are expected to cause some depolarization due to scattering. Secondly, the spatial variations across the sample (seen in Fig. 3d, e), combined with the finite beam radius at focus causes some degree of polarization variation. Lastly, while ambient light entering the polarimeter was minimized during experiments, it was not fully eliminated according to dark measurements performed where a beam block was placed between the objective and beam splitters. This was measured to account for about 7% out of the 11.6% depolarization at the resonance wavelength. As such, we do not expect significant depolarization from the polarization modulator itself.

Supplementary Note 17. Table of comparison across other devices

	Active Material	**Material thickness**	**Accessible parameter space**	**Tuning method**
Ref [10]	BP	40 nm	NIL. Polarimetry measurements	N.A.
Ref [11]	$MoSe_2$	Monolayer	Phase shift only	Electronic
Ref [12]	BP	9-14 nm	1D polarization azimuth angle	BP twist angle
Ref [13]	BP	1.59 nm	1D across Poincare sphere	Electronic
Ref [14]	MoS_2	41 nm	1D polarization azimuth angle	Thermo-optic
Ref [8]	Bulk ITO	5 nm	2D across Amplitude & Phase	Electronic
This work	BP	1.59 nm	2D patch on Poincare sphere	Electronic

Supplementary Table 1. Comparison of dual-gated BP device to other similar devices.

Supplementary Note 18. Cascading two single-gate devices in series

We consider an optical setup employing two identical single-gate devices along its optical path (Supplementary Fig. 18a). Assuming that the objective lenses and beam splitter do not affect the polarization state in any way, the second single-gate device is placed with its BP armchair axis oriented to maximally interact with the light reflected from the first device. The S_0 parameter denoting the optical efficiency is shown in supplementary fig. 18b. Due to the need for dual cavities in this setup, the overall reflected efficiency is approximately 20 dB lower than the dual-gated case.

The Poincare sphere coverage is also shown in supplementary fig. 18c. Here, the coverage is about half that of the dual-gated case. This is because the input polarization state into the second device is variable while the AC/ZZ axis of the device itself is fixed. If light is launched parallel to the inactive ZZ axis of the second device, then the second device loses its tunability. We attempted to minimize this by orienting the second device ZZ axis as far from the input polarization as possible, but the tunability still falls off with the input azimuthal angle as cos(ψ). Therefore, the 2 degrees of freedom in this system are partially coupled, which reduces overall tunability. Incorporation of both BP layers into a single cavity fully decouples the degrees of freedom, which allows a near-full Poincare sphere coverage.

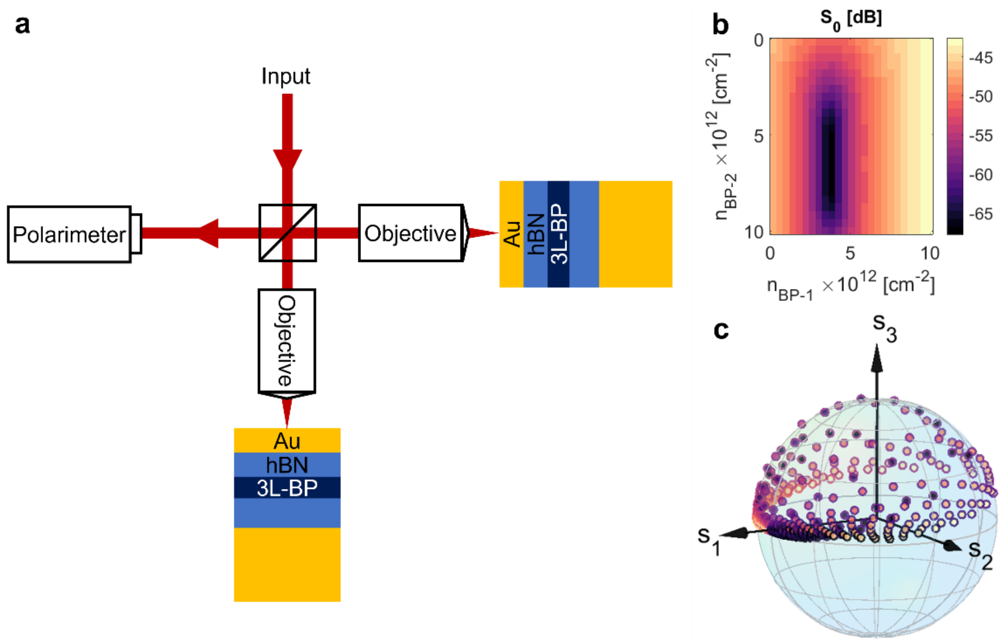

Supplementary Fig. 18. Analysis of cascading two single-gate devices. (**a**) Schematic of optical configuration cascading two single-gate devices. (**b**) S_0 parameter showing decreased optical efficiency due to dual-cavity configuration and beam-splitter for coupling. (**c**) Combined normalized Poincare sphere coverage when gating both devices in concert. Coverage is reduced to less than half of Fig. 1d because of partial coupling between the two degrees of freedom here.

In summary, a configuration employing two single-gate structures suffers from 20 dB poorer optical efficiency, poorer (<50%) polarization coverage due to partial coupling of the degrees of freedom, and a disadvantage in modularity and bulkiness due to the use of two separate devices compared to a single monolithic dual-gate structure demonstrated in this work.

Supplementary References

1. Liu, H.; Zhao, J.; Ly, T. H. Clean Transfer of Two-Dimensional Materials: A Comprehensive Review. *ACS Nano* **2024**, 18(18), 11573-11597.
2. Maniyara, R. A.; Rodrigo, D.; Yu, R.; Canet-Ferrer, J.; Ghosh, D. S.; Yongsunthon, R.; Baker, D. E.; Rezikyan, A.; Abajo, F. J. G.; Pruneri, V. Tunable plasmons in ultrathin metal films. *Nat. Photonics* **2019**, 13, 328-333.
3. Bennett, R. K. A.; Pop, E. How Do Quantum Effects Influence the Capacitance and Carrier Density of Monolayer MoS2 Transistors? *Nano Lett*. **2023**, 23(5), 1666-1672.
4. Awate, S. S.; Mostek, B.; Kumari, S.; Dong, C.; Robinson, J. A.; Xu, K.; Fullerton-Shirey, S. K. Impact of Large Gate Voltages and Ultrathin Polymer Electrolytes on Carrier Density in Electric-Double-Layer-Gated Two-Dimensional Crystal Transistors. *ACS Appl. Mater. Interfaces* **2023**, 15(12), 15785-15796.
5. Wu, K.; Zhong, H.; Guo, Q.; Tang, J.; Yang, Z.; Qian, L.; Yuan, S.; Zhang, S.; Xu, H. Revealing the Competition between Defect-Trapped Exciton and Band-Edge Exciton Photoluminescence in Monolayer Hexagonal WS_2. *Adv. Opt. Mater*. **2022**, 10, 2101971.

6. Tian, X.; Zheng, Q.; Jiang, X.; Zhao, J. Ab initio investigation on exciton-phonon interaction and exciton mobility in black phosphorene. *Phys. Rev. B* **2023**, 108, 245118.
7. Seah, S. K. W.; Biswas, S.; Hail, C. U.; Jang, M. S.; Atwater, H. A. Efficient, Polarization-Diverse State Generation with Tunable Black Phosphorus Cavity Heterostructures and Active Metasurfaces. *ACS Photonics* **2025**, 12(3), 1409-1417.
8. Park, J.; Jeong, B. G.; Kim, S. I.; Lee, D; Kim, J; Shin, C; Lee, C. B.; Otsuka, T; Kyoung, J.; Kim, S.; Yang, K. Y.; Park, Y. Y.; Lee, J.; Hwang, I.; Jang, J.; Song, S. H.; Brongersma, M. L.; Ha, K.; Hwang, S. W.; Choo, H.; Choi, B. L. All-solid-state spatial light modulator with independent phase and amplitude control for three-dimensional LiDAR applications. *Nat. Nano*. **2021**, 16, 69-76.
9. Novotny, L; Hecht, B. Propagation and focusing of optical fields. In: Principles of Nano-Optics. Cambridge University Press **2012**, 45-85.
10. Xiong, Y.; Wang, Y.; Zhu, R.; Xu, H.; Wu, C.; Chen, J.; Ma, Y.; Liu, Y.; Chen, Y.; Watanabe, K.; Taniguchi, T.; Shi, M.; Chen, X.; Lu, Y.; Zhan, P.; Hao, Y.; Xu, F. Twisted Black Phosphorus–based van der Waals Stacks for Fiber-integrated Polarimeters. *Sci. Adv.* **2022**, 8, eabo0375.
11. Li, M.; Biswas, S.; Hail, C. U.; Atwater, H. A. Refractive Index Modulation in Monolayer Molybdenum Diselenide. *Nano. Lett.* **2021**, 21(18), 7602-7608.
12. Wang, S.Y.; Huang, K.X.; Guo, Q.Q.; Guo, H.W.; Tian, J.G.; Liu, Z.B. Tunable Optical Rotation in Twisted Black Phosphorus. *J. Phys. Chem. Lett*. **2021**, 12, 4755-4761.
13. Biswas, S., Grajower, M. Y., Watanabe, K., Taniguchi, T., Atwater, H. A., Broadband Electro-optic Polarization Conversion with Atomically Thin Black Phosphorus. *Science* **2021**, 374, 448-453.
14. Ahmad, H.; Lim, H.S.; MatJafri, M.Z.; Ge, Y.Q.; Zhang, H.; Tiu, Z.C. All-fiber optical polarization modulation system using MoS2 as modulator. *Infrared Phys. Tech*. **2019**, 102, 103002.